Virus Research 323 (2023) 198995

Contents lists available at ScienceDirect

Virus Research

journal homepage: www.elsevier.com/locate/virusres

# A new host-targeted antiviral cyclolignan (SAU-22.107) for Dengue Virus infection in cell cultures. Potential action mechanisms based on cell imaging☆

Yaneth M. Brand [a,b], Vicky Roa-Linares [a,b], Carolina Santiago-Dugarte [c], Esther del Olmo [c], José Luis López-Pérez [c,d,*], Liliana Betancur-Galvis [a,b], Juan Carlos Gallego-Gómez [b,*], Arturo San Feliciano [c,e]

[a] Group of Investigative Dermatology, Institute of Medical Research, Faculty of Medicine, University of Antioquia, Medellín, Colombia
[b] Translational and Molecular Medicine Group, Institute of Medical Research, Medicine Faculty, University of Antioquia, Medellín, Colombia
[c] Departamento de Ciencias Farmacéuticas, Área de Química Farmacéutica, Facultad de Farmacia, CIETUS, IBSAL. Campus Miguel de Unamuno, University of Salamanca, 37007, Salamanca, Spain
[d] Facultad de Medicina, Universidad de Panamá, Panamá, R. de Panamá
[e] Programa de Pós-graduação em Ciências Farmacéuticas, Universidade do Vale do Itajaí, UNIVALI, Itajaí, SC, Brazil

ARTICLE INFO

*Keywords:*
Dengue
Host-targeted antiviral
Cytotoxicity
Microtubule
Endoplasmic reticulum, and cyclolignan

ABSTRACT

Dengue virus (DENV) infection is the most arbovirosis in the world. However, medications have not been approved for its treatment. Drug discovery based on the host-targeted antiviral (HTA) constitutes a new promising strategy, considering their high genetic barrier to resistance and the low probability of selecting drug resistance strains. In this study, we have tested fifty-seven podophyllotoxin-related cyclolignans on DENV-2 infected cells and found the most promising compound was S.71. Using cellular and molecular biology experiments, we have discovered that the new lignan altered the distribution of microtubules, induced changes in cell morphology, and caused retraction of the rough endoplasmic reticulum. In addition, the compound alters the viral envelope protein and the double-stranded RNA, while there is a decrease in negative-strand RNA synthesis; especially when the compound was added between 6- and 12-hours post-infection. Altogether, S.71 decreases the viral yield through an HTA-related mechanism of action, possibly altering the DENV genome replication and/or polyprotein translation, through the alteration of microtubule distribution and endoplasmic reticulum deterioration. Finally, pharmacokinetic predictors show that S.71 falls within the standard ranges established for drugs.

## 1. Introduction

DENV is a mosquito-borne flavivirus of global public health importance, with an annually estimated 390 million infections (Dengue y dengue grave 2021). DENV is a positive-sense, single-stranded RNA enveloped virus whose genome encodes three structural proteins and seven non-structural proteins. Although dengue infections have high morbidity and mortality, there are no antiviral therapies approved against this virus. DENV, like the other flaviviruses, exploits the cytoplasmic cellular machinery and interacts with membranes and biochemical processes of host cells to facilitate its replicative cycle (Greber and Way, 2006).

Microtubules (MTs) have been involved in the replication cycle of DNA and RNA viruses (Shrivastava et al., 2011) and participate in the traffic flaviviruses (Shrivastava et al., 2011). MTs are structures composed of heterodimeric subunits of α- and β-tubulin that radiate throughout the cell (Karp, 2009). Microtubule dynamics and their control are essential for the maintenance of morphology and support of organelles such as the endoplasmic reticulum (Karp, 2009).

The endoplasmic reticulum (ER) is a multifunctional signaling organelle that controls a wide range of cellular processes, including protein synthesis (Karp, 2009). The ER is a membranous system that is connected to the microtubules; for this reason, these structures are interdependent (Karp, 2009). Several studies identified the ER as the

☆ *In Memoriam,* to Prof. Dr. Mahabir P. Gupta

* Corresponding authors.
*E-mail addresses:* jose.lopezp@up.ac.pa (J.L. López-Pérez), carlos.gallego@udea.edu.co (J.C. Gallego-Gómez).

https://doi.org/10.1016/j.virusres.2022.198995
Received 6 July 2022; Received in revised form 31 October 2022; Accepted 31 October 2022
Available online 4 November 2022

cellular compartment where translation (Gillespie et al., 2010), replication (Gillespie et al., 2010), and maturation processes of flaviviruses occur (Chatel-Chaix and Bartenschlager, 2014; Reid et al., 2018). During infection, flaviviruses promote the formation of specialized compartments known as RCs (replicative complexes), which are described as the remodeling of ER. These membranous structures: vesicular packages (VPs) and convoluted membranes (CM) provide a microenvironment necessary for the coordination of different stages of the dengue replicative cycle, specifically RNA replication, protein translation, and virus assembly (Gillespie et al., 2010; Chatel-Chaix and Bartenschlager, 2014; Reid et al., 2018; Paul et al., 2011; Mackenzie, 2005). Considering the above, it is interesting to study molecules with effects against MTs and ER required for the replicative cycle of dengue and other RNA viruses.

Lignans, including derivatives and analogs, are a large family of natural aromatic polyoxygenated compounds that have demonstrated diverse types of bioactivity, while some of them have attained approval as drugs for clinical use, mainly as anticancer and particularly as antiviral agents (Ayres and Loike, 1990, Petersen et al., 2010, Cunha et al., 2012, Zálešák et al., 2019, Xu et al., 2009 and Cui et al., 2020). Podophyllotoxin (POD) (Fig. 1), a cyclolignan, is a potent antimitotic that has the ability to inhibit tubulin polymerization. POD was approved for clinical use against condyloma acuminata, caused by papillomavirus (Bertolotti et al., 2020 and Attiaa et al., 2015), and is also a drug lead and starting substrate for the synthesis of several approved anticancer drugs (Gordaliza et al., 2004, Montecucco et al., 2015, Hande et al., 1998).

POD and related lignans are effective against Herpes and other viruses (Gordaliza et al., 1994, Sudo et al., 1998, Cohen et al., 2016), suggesting their evaluation to other viruses. Thus, from a library of hundreds of natural and hemisynthetic lignans obtained in our laboratories, an antiviral screening against DENV was performed. Considering antiviral potency and lower cytotoxicity, the lactonic cyclolignan 7-deoxy-7β-(2-methylprop-1-enyl) picropodophyllotoxin (Hernández et al., 2018; Abad et al., 2012), encoded as S. 71 (Fig. 1) was selected for antiviral mechanisms studies, in parallel with POD.

In order to characterize the antiviral profile of S.71, we determined its biological effects, complemented with computational models for analyzing its interaction with tubulin, and also for predicting its pharmacokinetic properties that were evaluated by Lipinski's Rule of Five, this describes properties as hydrophobicity, electronic distribution, hydrogen bonding characteristics, molecule size, flexibility, bioavailability, transport properties, affinity to proteins, reactivity, toxicity, metabolic stability, and many others (Friesner et al., 2004, Friesner et al., 2006, Halgren et al., 2004, Elmore, 2007; Sultana et al., 2018).

In general, Lipinski's Rule of Five consists in:

- Not more than 5 hydrogen bond donors (OH and NH groups)
- Not more than 10 hydrogen bond acceptors (notably N and O)
- A molecular weight under 500 g/mol
- A partition coefficient log *P* less than 5 (lipophilicity)

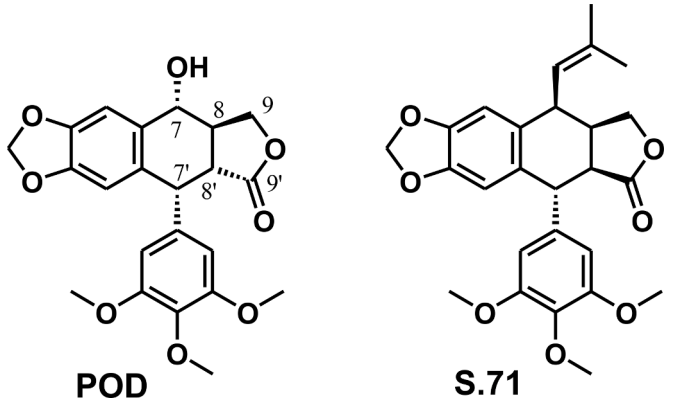


**Fig. 1.** Structures of podophyllotoxin (POD) and the new anti-DENV cyclolignan SAU-22.1071 (S.71).

The results demonstrated that S.71 has molecular properties and structural features similar to the known drug "drug-likeness" and decreases the viral yield by an HTA-related mechanism of action through the alteration of MTs and ER distribution, disturbing the configuration of the viral factories. Finally, computational predictions showed that the new anti-DENV compound has drug-likeness properties.

## 2. Methodology

### 2.1. Reagents, medium, and antibodies

Dimethyl Sulfoxide (DMSO), MTT [3-(4,5-dimethylthiazol-2-yl)−2,5 diphenyltetrazole], Dulbecco's Modified Eagle's Medium (DMEM), and the X-tremeGENE HP DNA Transfection Reagent were purchased from Sigma-Aldrich (St Louis, USA). Fetal Bovine Serum (FBS) and the antibiotic Penicillin-Streptomycin-Neomycin (PSN) were obtained from Invitrogen (Carlsbad-California, USA) and ribavirin was purchased from Calbiochem. Primary antibodies: antibody mAB anti-α/β-tubulin (TU-10, Invitrogen ™), the anti-ENV produced in hybridoma 4G2 cells, anti-dsRNA antibody (J2, Scicons') and anti-gamma tubulin antibody (ab11317, Abcam) were used. Secondary antibodies: Alexa Fluor 594 (Goat anti-mouse IgG H&L) and Alexa Fluor 488 (Goat anti-mouse and Anti-rabbit IgG H&L) were used. Nucleus staining was performed with Hoechst 33,342 (Molecular Probes®).

### 2.2. Antiviral assays

#### 2.2.1. Cytotoxicity assay

The effect of S.71 and POD on cell viability was evaluated using the MTT technique according to Roa-Linares et al., 2016 (Roa-Linares et al., 2016).

The $CC_{50}$ value (Cytotoxic Concentration 50%) for the compounds was obtained by linear regression analysis of concentration-response curves using GraphPad Prism 5.0 statistical program. $CC_{50}$ values were expressed as mean ± the standard deviation ($M \pm SD$) of two independent experiments performed in triplicate (Roa-Linares et al., 2016).

#### 2.2.2. Inhibition of dengue virus DENV-2 in pre-infection and post-infection stages

S.71 was evaluated on pre-infection and post-infection stages, using a concentration of the determined $CC_{50}$. To assess the activity of the compound on virus adherence, a mixture of DENV-2 (Multiplicity of Infection, MOI=1 PFU/cell, PFU: Plaque forming units) with different dilutions of the compound (12.5–100 μM) was added to the cells. Later, cells were incubated for 1 h at 4 °C; then, the mixture was removed, washed with cold PBS, and carboxymethylcellulose (CMC) 1.5% was added (Roa-Linares et al., 2016).

To determine the efficacy of S.71 against virus entry, cells were pretreated with the compound (12.5–100 μM) for 24 h at 37 °C. Subsequently, the treatment was removed, and the cells were washed with PBS to be infected with MOI=1. Then, cells were incubated for 2 h at 37 °C; finally, the inoculum was removed to add 1.5% CMC (Roa-Linares et al., 2016).

For the post-infection stage, cells were infected with MOI=1 and incubated for 2 h at 37 °C (5% $CO_2$) and wells were washed with PBS and the compound solutions (12.5–100 μM), previously prepared in 1.5% CMC medium were added (Roa-Linares et al., 2016). For each assay, logarithmic dilutions of POD (0.1 - 100 μM) were used as a positive control.

All experiments were incubated for 6 days, and viral plaque counting was performed in 3 independent assays to determine the inhibition of the plaque-forming unit (PFU/mL) (Roa-Linares et al., 2016). Likewise,

the effective concentration ($EC_{50}$) was defined as the concentration that reduces viral plaques by 50%.

### 2.3. Studies focused on the antiviral mechanism of action

#### 2.3.1. Time-of-addition (TOA) assay

Cells were infected with MOI=1 and incubated for 2 h at 37 °C, (5% $CO_2$). Wells were washed with PBS and DMEM (2% FBS) containing the active concentration of S.71 (72.4 μM) or POD (0.1 μM) were added after 6, 12, 24 and 36-hours post-infection (hpi) (Cardozo et al., 2011), and incubated for a further 24 h. Later, the supernatants were harvested and titrated by the PFU assay.

#### 2.3.2. Effects of S.71 on cellular and viral components

To assess the effects of the compounds on microtubules, BHK-21 cells were seeded on coverslips and subsequently infected with MOI=1 for 2 h. After 6 and 12 hpi, solutions of S.71 (72.4 μM) or POD (0.1 μM) were added. After 24 h of treatment, viral supernatants were collected to be titrated for PFU/mL. Finally, the cells were washed with cytoskeleton buffer and fixed with 3.8% paraformaldehyde, in order to use and label protocol to ENV protein, dsRNA, MTOC, and nuclei (Martinez-Gutierrez et al., 2011). Additionally, BHK-21 cells were transfected with the pmKate2-ER plasmid using Sigma's Xtreme gene hp DNA (Evrogen pmKate2-ER (CAT.# FP324) 2018). After 24 h post-transfection, cells were infected with a MOI=1, and after 6 and 12 hpi they were treated as mentioned above. Finally, the coverslips were observed in a spinning-disk confocal microscope (Olympus IX-81 DSU) and epifluorescence microscope (60X objective); images were processed by Image J software.

#### 2.3.3. Effect of S.71 on the production of negative-strand rna

Total RNA was extracted from cells infected through phenol-chloroform. Then the synthesis of the cDNA antigenome of DENV-2 was performed using SuperScript™ III Reverse Transcriptase kit of Thermo Fisher Science - US and forward primer 5 'CAATATGCTG AAACGCGAGAGAAA. The viral copy number was estimated by qPCR using primers previously reported: The DENV-2-specific primers (forward: 5′ CAATATGCTGAAACGCGAGAGAAA 3′ and reverse: 5′CCCCATCT ATTCAGAATCCCTGCT 3′) and el kit Maxima SYBR Green qPCR Master Mix de Thermo Fisher Scientific-US (Castillo et al., 2016).

### 2.5. Characterization of cellular integrity during DENV-2 infection and treatment

#### 2.5.1. Annexin v staining, size, and granularity evaluation

BHK-21 cells previously treated and infected were resuspended in a binding buffer solution and annexin V. The mixture was incubated for 15 min at 4 °C; then, the binding buffer was added to be centrifuged for 5 min. Finally, samples were analyzed on a cytometer (BD Facs Canto II, by Becton Dickinson) (Castellanos et al., 2016). Additionally, the complexity (size and granularity) of the infected and treated cells was determined, considering the parameters FSC (Forward Scatter) and SSC (Side Scatter).

#### 2.5.2. Cell recovery assays

Cells previously seeded on coverslips were treated and exposed for 24 h to treatment with S.71 or POD. Later, the compounds were removed and the cellular monolayers were washed. Next, DMEM 2% FBS was added and they were incubated for 3 days. After, the cells were washed and fixed as previously described for labeling of the nuclei. The coverslips were observed in a confocal microscope.

### 2.6. In silico studies

#### 2.6.1. Molecular docking

Docking calculations were performed using Glide (Friesner et al., 2004, Friesner et al., 2006, Halgren et al., 2004) integrated into the Schrödinger Molecular Modelling Suite. The tubulin-podophyllotoxin complex from *Bos taurus* (PDB:1SA1) was selected as the target. The complex was processed with the Protein Preparation Wizard. Finally, the model was refined using OPLS-2005 Force Field. POD and S.71 were processed with the LigPrep before optimizing the structure of each ligand (Friesner et al., 2004, Friesner et al., 2006, Halgren et al., 2004).

A receptor grid was centered in the ligand-binding site of the tubulin complex. Docking was carried out using the Extra Precision (XP) mode of Glide. The final poses were selected using the energetic parameter XPGlideScore function (Friesner et al., 2004, Friesner et al., 2006, Halgren et al., 2004).

#### 2.6.2. Prediction of pharmacokinetic parameters

The OSIRIS platform was used (Elmore, 2007) for toxicity and drug-likeness assessment, and SwissADME (Sultana et al., 2018) for predicting physicochemical parameters related to Lipinski's rule of five, bioavailability, and metabolism.

## 3. Results

### 3.1. S.71 is active against DENV-2 in the post-infection stages

The $CC_{50}$ on BHK-21 cells showed that S.71 was 166.7 μM and the POD compound was very toxic at concentrations >1 μM, but below this concentration, POD was cytostatic; ie, the treatment stops the growth of cells without killing them. For this reason, the $CC_{50}$ could not be determined. (Fig. S2). For this reason, the 57 cyclolignans were evaluated at 1–100 μM concentrations range (Table ST1), highlighting that S.71 showed relevant antiviral results with lower toxicity. S.71 was not active in the early stages of the DENV-2 replicative cycle (Fig. S3). However, this compound showed inhibition on post-infective stages with an $EC_{50}$ of 72.4 μM (Fig. 2)

As shown in Fig. 2, significant decreases in the viral titer after S.71 treatment at 50 and 100 μM for six days were observed. The positive control POD was effective at 0.1 μM.

### 3.2. Effects of S.71 and pod on viral yield and negative-strand rna synthesis

A one-step growth curve was standardized to know the growth kinetics of DENV-2 (Fig. S4). We observed the viral entry occurs at 2hpi, the viral eclipse at 6 to 12 hpi, and the viral egress at 24 post-infection (hpi). It is relevant to highlight that in the viral eclipse phase, viral protein translation, viral genome replication, and viral assembly take place. Considering the above, the TOA experiment (single replication cycle) was performed, and thus, S.71 and POD were added after 6, 12,

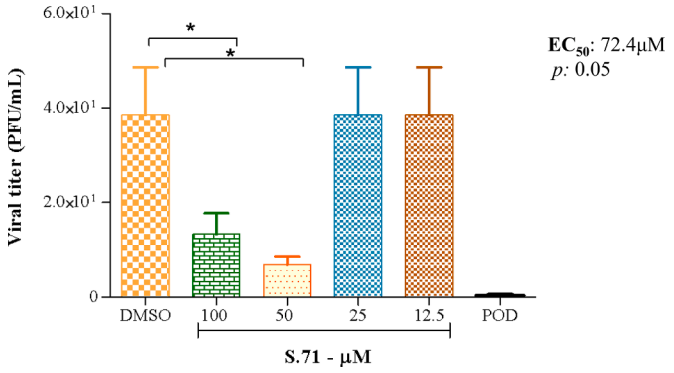


**Fig. 2. Antiviral results for S.71 and POD in post-infection stages of DENV-2 BHK-21 cells infected with MOI=1.** The bars represent means and standard deviations relative to control and p values were determined using the Student's *t*-test of unpaired data. DMSO <0.05% in all tests. POD (0.1 μM).

24, and 36 (hpi).

The viral yield was defined as a viral progeny obtained when the viral cycle has been completed and was evaluated by PFU assay. To understand the first step toward viral replication, we examined the DENV minus-strand RNA because this strand serves as a template for the amplification of additional positive-strand genomic RNA. Since the viral replication is ER-associated and this organelle is connected to the microtubules, the effect of the S.17 and **POD** was evaluated.

S.71 significantly reduced the yield of DENV-2 (Fig. 3A), as well as the negative-strand RNA copies at 6 and 12 hpi (Fig. 3B) in comparison with untreated controls. Also, S.71 altered the cellular morphology of mock-infected (cells without infection) and infected cells (Fig. 3C).

### 3.3. S.71 alters microtubules, dsRNA, and env protein distribution without affecting the mtoc

To validate the tubulin-related mechanism of action of S.71 and POD, we analyzed the microtubules distribution on infected and treated cells (Figs. 4 and 5).

BHK-21 cells have an elongated and fibroblastic-like phenotype, and microtubules appear as fine and thin fibers. Notably, infected and uninfected cells treated either at 6 or 12 hpi showed an atypical polygonal form and microtubule distributed separately after S.71 treatment. During POD treatment, cells showed a round morphology and fragmented microtubules (Figs. 4A and 5A).

Furthermore, on S.71 and POD-treated cells after 6 hpi (Fig. 4) and 12 hpi (Fig 5), the mean fluorescence intensity (MFI) of viral elements, such as dsRNA (Fig 4B, and Fig 5B) and ENV protein (Fig. 4C and Fig. 5C), were quantified. In untreated cells, dsRNA was distributed in a thick and compact granular pattern limited to the perinuclear area (Figs. 4A and 5A); meanwhile, the ENV protein is visualized as fine granules throughout the area of the cell (Figs. 4A and 5). On the other hand, in treated cells, significant decreases in dsRNA (Figs. 4B and 5B) and ENV protein signals (Figs. 4C and 5C) were detected. Additionally, the dsRNA distribution was observed to be distant from the perinuclear area (Figs. 4A and 5A).

Considering the importance of the microtubule organizing center (MTOC) for the nucleation of microtubules, the localization of this structure was examined. On mock and cells treated with S.71, the MTOC was observed as a point located in the perinuclear area. However, in cells treated with POD and with nocodazole, the MTOC was not detected (Fig. 6). MTOC quantification in S.71-treated cells revealed that for every three cells in the field, two had the typical morphology of this structure (2:3 ratio), while the cells treated with POD presented a 1:3 ratio.

### 3.4. The S.71 treatment changes the distribution of the rough endoplasmic reticulum

The treatments with S.71 and POD, either 6 hpi (Fig. 7A, arrows) or 12 hpi (Fig. 7B), induced the ER retraction on infected and mock cells (Fig. S5). This phenomenon is probably related to the changes in the distribution pattern of MTs during exposure to such treatments.

### 3.5. S.71 increased cell granularity and did not affect the cell size nor induce phosphatidylserine exposure

Cells treated with the lignans showed alterations; therefore, it was necessary to clarify whether the observed morphological changes could represent early events of cell death. Significantly, when infected or uninfected BHK-21 cells were exposed to treatments with S.71 and POD for 24 h, changes in cell size were not observed (Figs. 8A and D), nor changes in phosphatidylserine exposure (Figs. 8C and F). However, an increase in cell granularity was detected (Figs. 8B and E).

### 3.6. The S.71 effects on cell morphology are reversible

Considering the toxic effects of lignans, the recovery of cell morphology after treatment removal was determined. Untreated BHK-21 cells showed an elongated three-dimensional morphology, whereas,

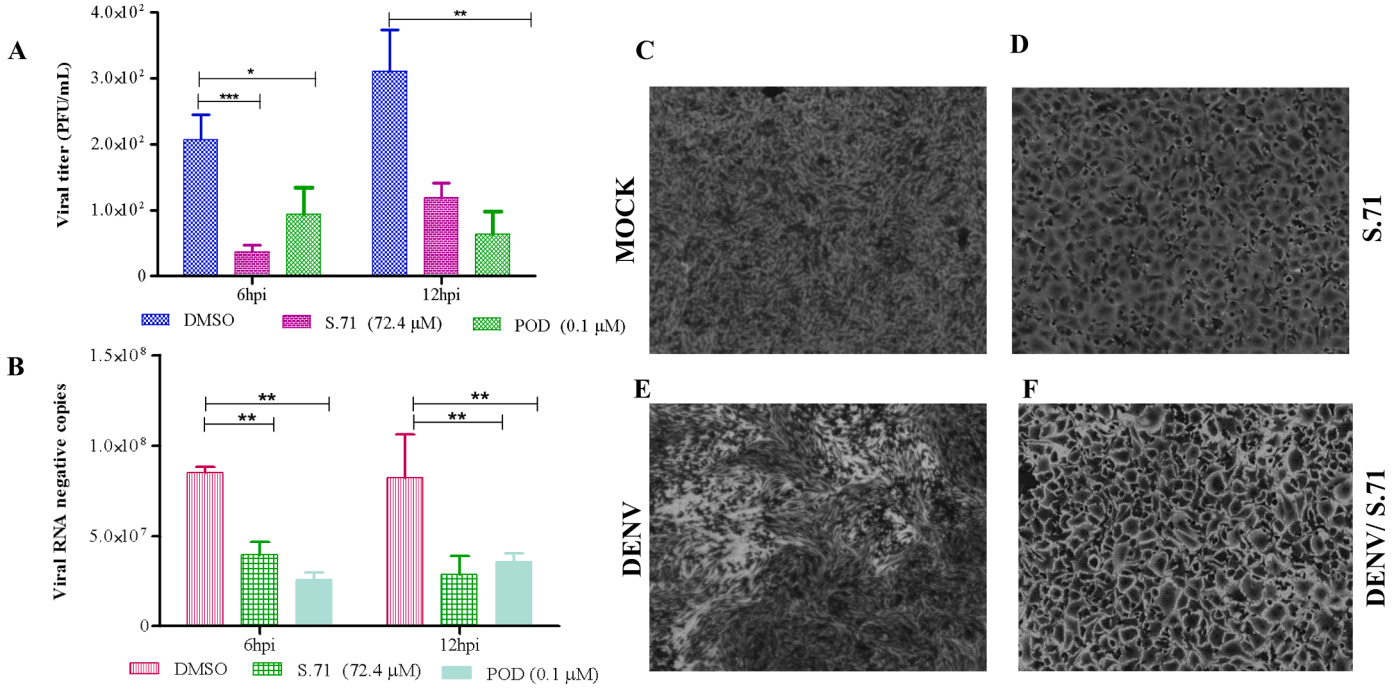


**Fig. 3. Effects of S.71 and POD on viral yield (A), negative-strand RNA synthesis (B), and morphology of cells without infection (C), cells treated with S.71 (D). Moreover, was observed cells infected (E) and cells infected/treated with S.71 (F). BHK-21 cells were infected with MOI=1 and cells were exposed for 24 h to the compounds.** The bars represent the mean ± s.e.m of three independent experiments. The DMSO concentration was <0.05%. (*): $p$ <0.05; (**): <0.01; (***): <0.001. The comparison between groups was performed using the one-way ANOVA test.

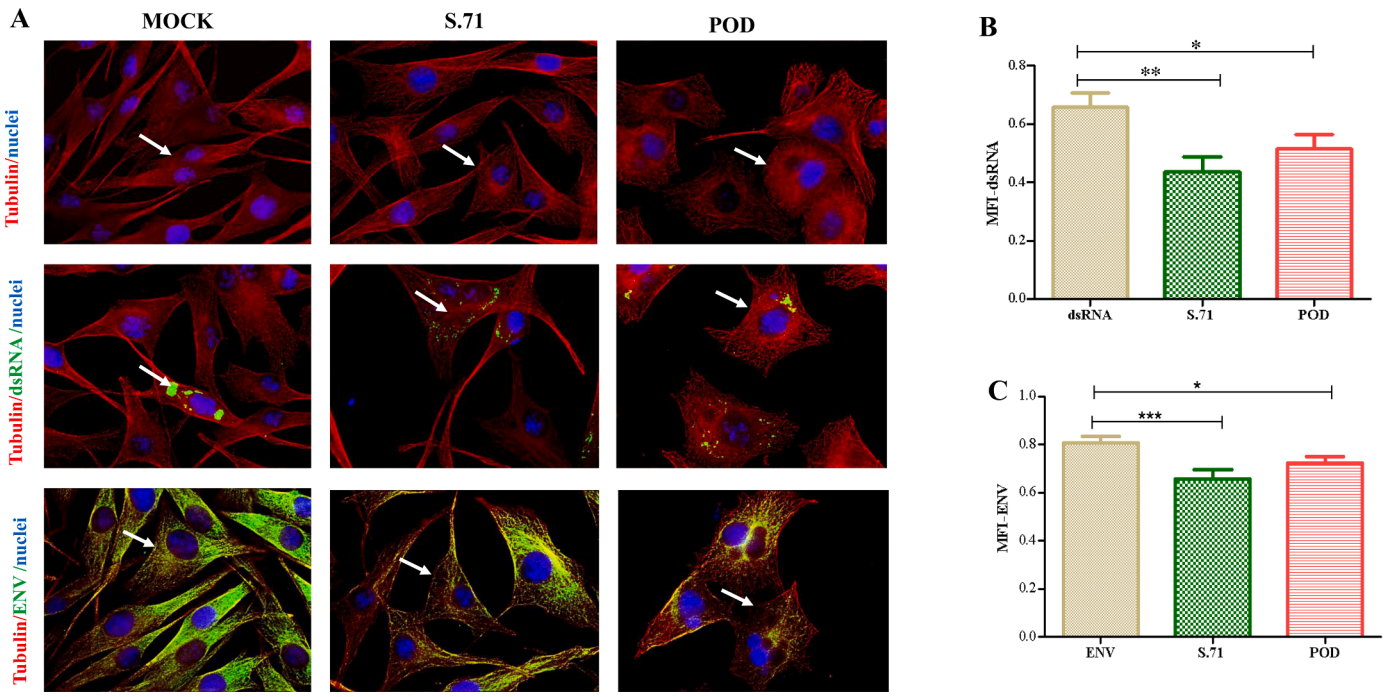


**Fig. 4. Effects of S.71 and POD on microtubules during** 24 h **exposition (A), dsRNA (A, B), and viral envelope protein (A, C) distributions when added at 6 hpi on BHK-21 cells infected with MOI=1**. Pictures were captured with a 60X objective. Graphs represent the quantification of the mean fluorescence intensity (MFI) of dsRNA (B) and ENV protein (C) and correspond to three independent triplicate experiments. Microtubules (red), dsRNA, and envelope protein ENV (green) and nuclei (blue) - see arrows. (*): p values <0.05; (**) <0.01; (***): <0.001, were determined using the Student's-T-test of unpaired data.

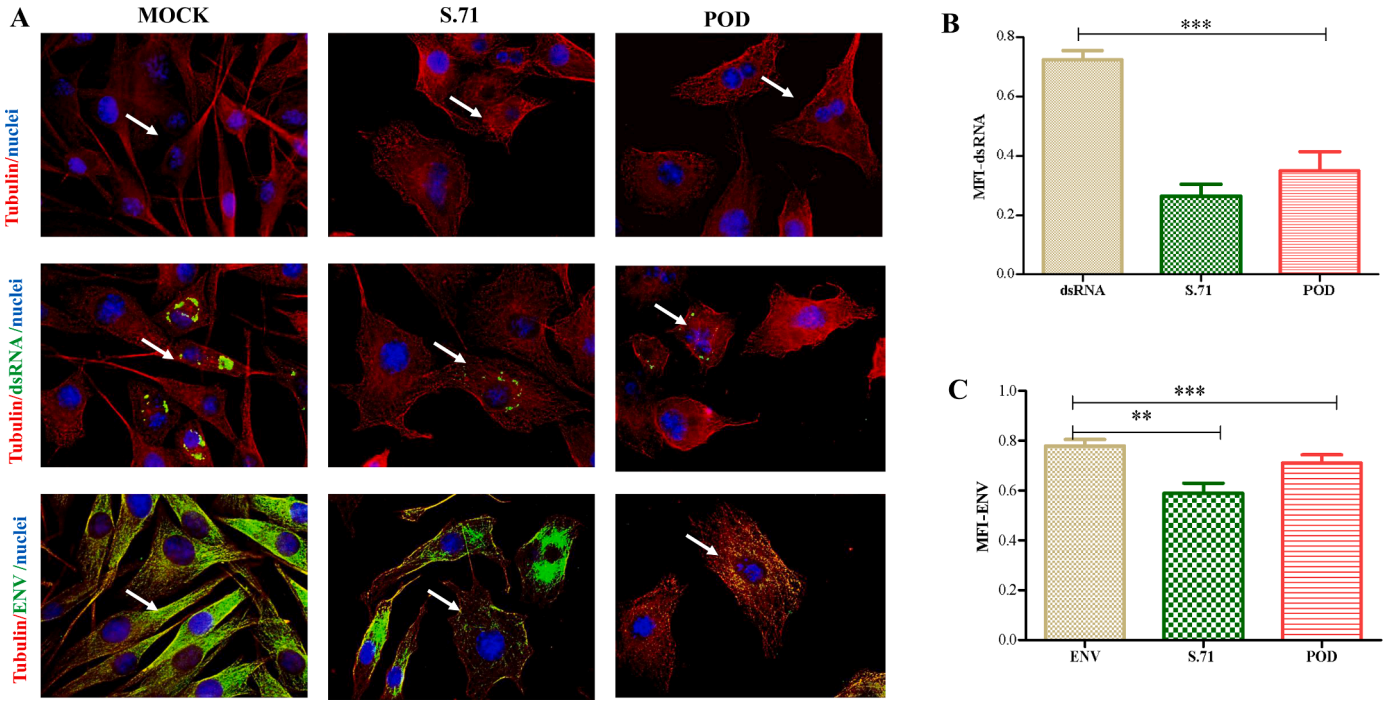


**Fig. 5. Effects of S.71 and POD on microtubules during** 24 h **exposition (A), dsRNA (A, B), and viral envelope protein (A, C) when added at 12 hpi on infected BHK-21 (MOI=1).** Quantification of the mean fluorescence intensity (MFI) for dsRNA (B) and ENV protein (C) is shown. Pictures were captured with a 60x objective and graphs correspond to three independent triplicate experiments. Microtubules (red), dsRNA, and envelope protein ENV (green) and nuclei (blue) - see arrows.

after treatment with S.71 and POD for 24 h, the shape of the cells became flat, polygonal, or round (Fig. 9A). Cells treated with POD showed pyknotic and fragmented nuclei, while such degradation was not observed on the cells treated with S.71. When the treatment was removed and replaced with a nutrient-supplemented medium, the cells recovered their normal morphology after three days (Fig. 9B).

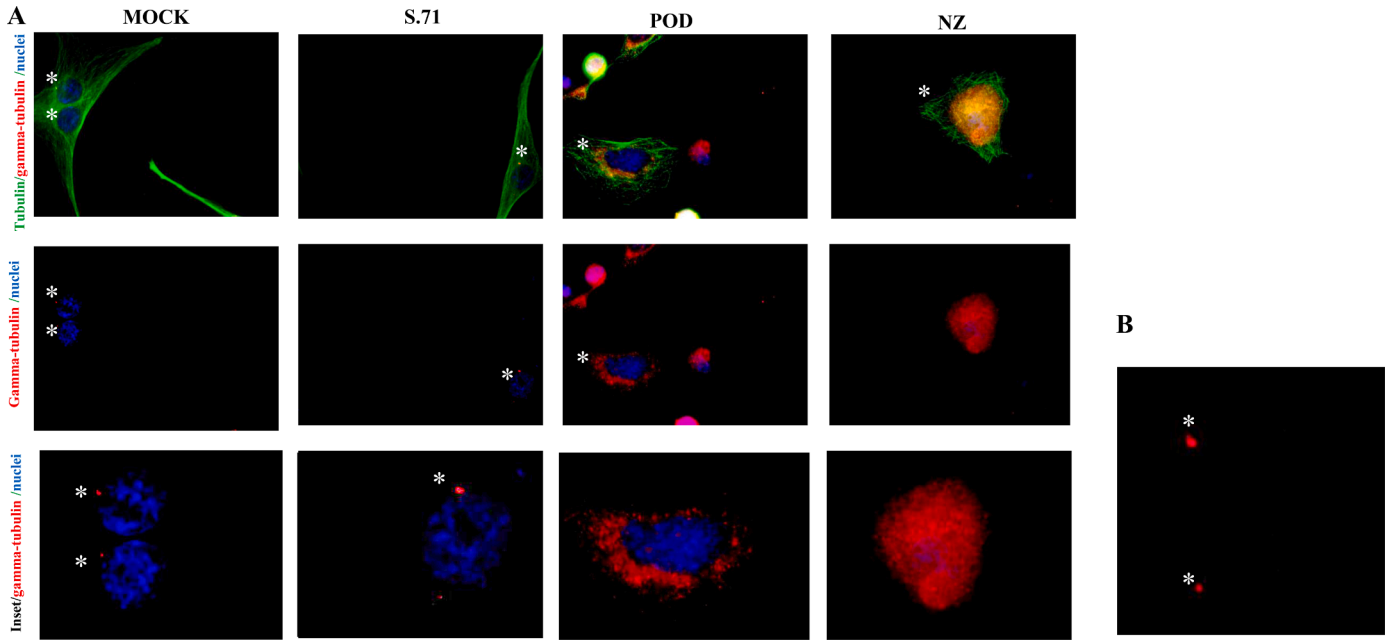


**Fig. 6. Effects of S.71, POD, and nocodazole (NZ) on the microtubule-organizing center (MTOC) of BHK-21 cells after** 24 h **treatment (A). Image B corresponds to the MTOC enlargement. There is a noteworthy presence of MTOC in MOCK and S.71, contrary to their absence in the treatment of POD and NZ.** Microtubules (green), MTOC (red), and nuclei (blue). Asterisks indicate the MTOC localization.

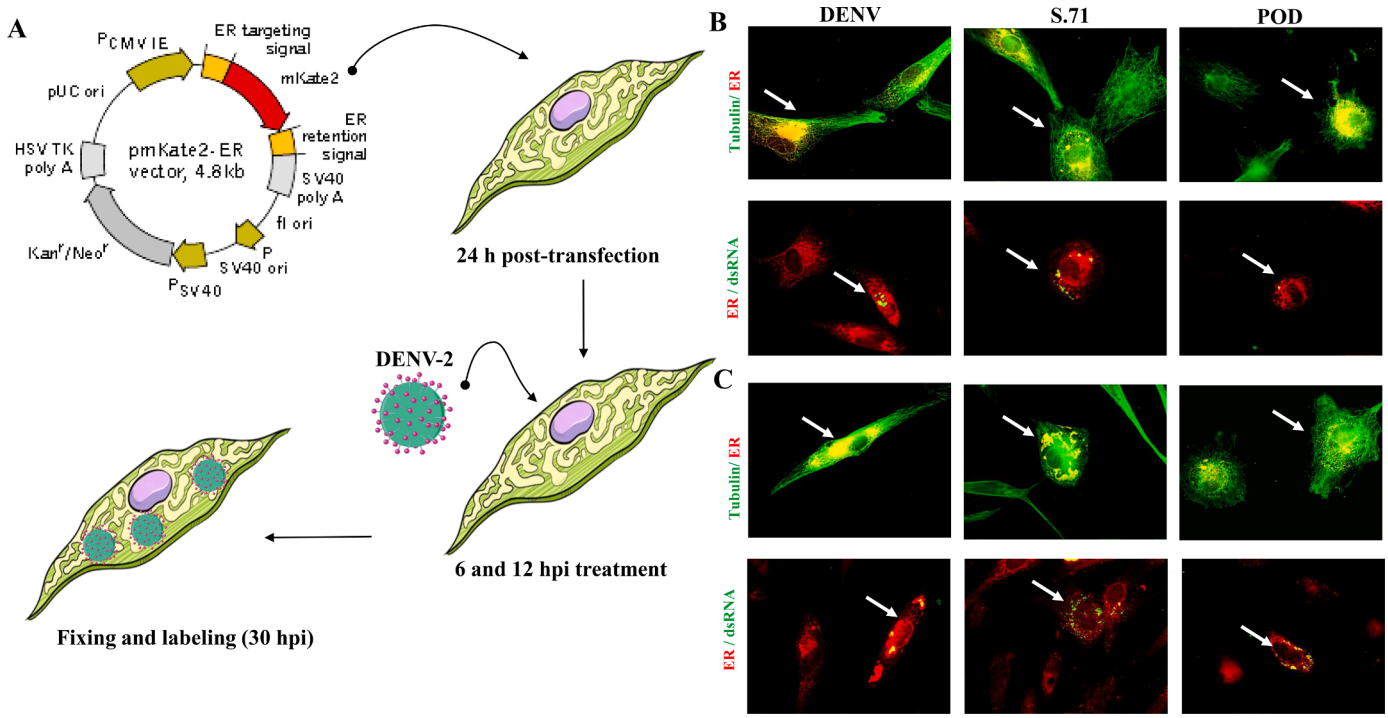


**Fig. 7. Effects of S.71 and POD on rough endoplasmic reticulum (ER) on infected BHK-21 (MOI=1).** The workflow shows the obtention of transfected cells with ER (A). Microtubules, ER, and dsRNA **(B, C)** distributions in ER-transfected BHK-21 cells, after treatments initiated at 6 **(B)** and 12 **(C)** hpi. Pictures show microtubule distribution (green), and expressions of ER (red) and dsRNA (green) - see arrows. Images captured with a 60x objective correspond to one of three independent triplicate experiments.

### *3.7. S.71 interacts with tubulin subunits*

Both ligands dock in the same site (Fig. 10), but the spatial orientation is different due to the rigidity of the *trans*-fused lactone system in POD *versus* the more flexible *cis*-fused of S.71. Such flexibility allows the cyclohexene ring of the molecule to adopt a boat conformation combined with the pseudo-equatorial orientation of the 7β-isobutenyl substituent at C-7 (Fig. 1).

In the 2D-maps, the docking contacts of POD (Fig. 11A) and S.71 (Fig. 11B) can be analyzed. The main interactions for these cyclolignans correspond to the H-bonds marked by arrows, being of type H-donor for the hydroxyl group of POD towards the Thr179 residue of the tubulin

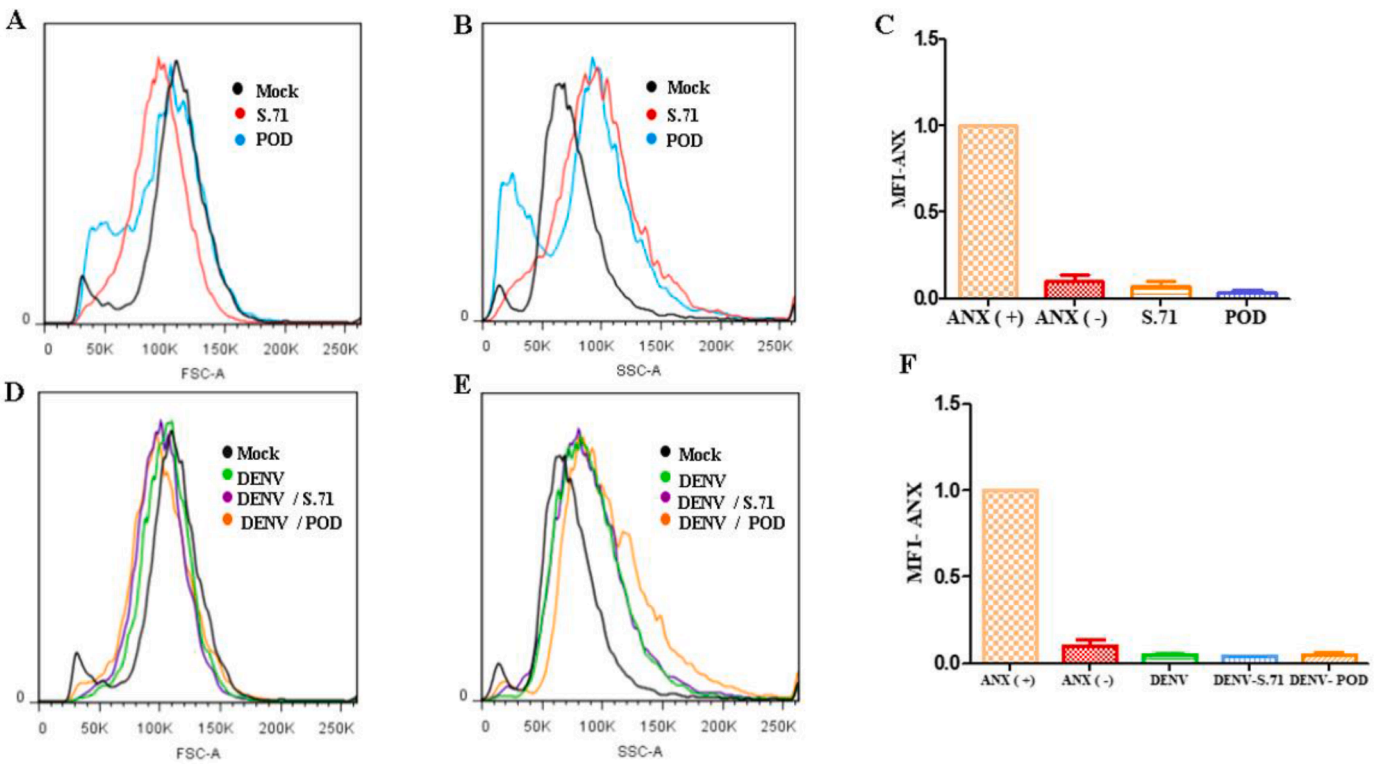


**Fig. 8. Effects of S.71 and POD on cell size (A, D) and granularity (B, E) and induction of phosphatidylserine exposure in mock (A-C) and infected (D-F) BHK-21 cells (MOI=1)..** Treatments with S. 71 and POD did not substantially alter the size (A) but increased the granularity of normal cells (B). S.71, and POD also did not generate phosphatidylserine exposure (C) after 24 h. The results were similar for infected cells (E- F).

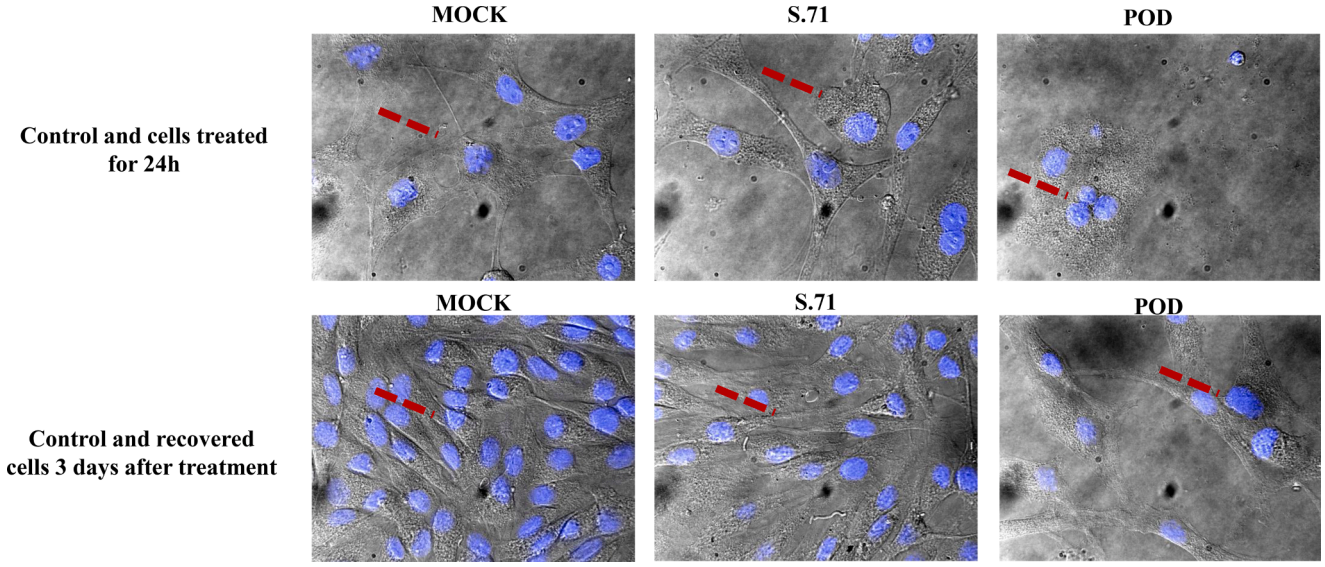


**Fig. 9. Effects of S.71 and POD on cell morphology after a 24 h treatment and recovery after three days.** Images were obtained with differential interference contrast and a 60x objective, and nuclei were labeled in blue. Dotted lines reveal morphological changes in treated cells.

α-subunit, whereas the 1,3-dioxole fragment of S.71 acts as H-acceptor from the Lys352 β-subunit residue. Lys352 is also a positively charged contact for POD, while Lys254 acts similarly for S.71. Most other contacts are of a hydrophobic (green) or polar (blue) nature.

### 3.8. Toxicity risks, drug-likeness, and adme properties

The Osiris predictor (Evrogen pmKate2-ER (CAT.# FP324) 2020) assigned no mutagenic, tumorigenic, or irritant risks for either S.71 or POD, while the potential effects on cell cycle were predicted for both compounds, to which the drug-likeness/drug-score values of 3.84/0.29 and 4.19/0.45 were respectively predicted. The SwissADME predictor (1. Sultana et al., 2018) showed that S.71 and POD meet the conditions defined in Lipinski's rule of five, and estimated high gastrointestinal absorption with a bioavailability factor of 0.55 for both compounds (Table ST2).

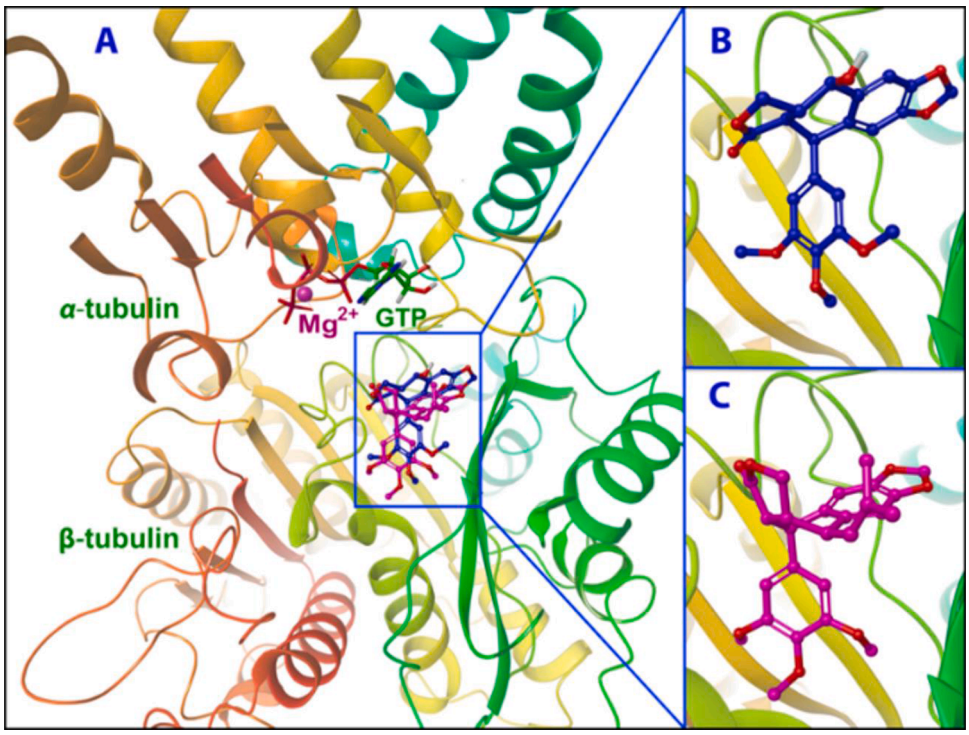


**Fig. 10.** Superimposition of POD (blue) and S.71 (purple) as docked in the colchicine site of the α-β tubulin heterodimer, with GTP and $Mg^{2+}$ associated with the α-tubulin subunit (A), and complexes of **POD** (B) and S.71 (C).

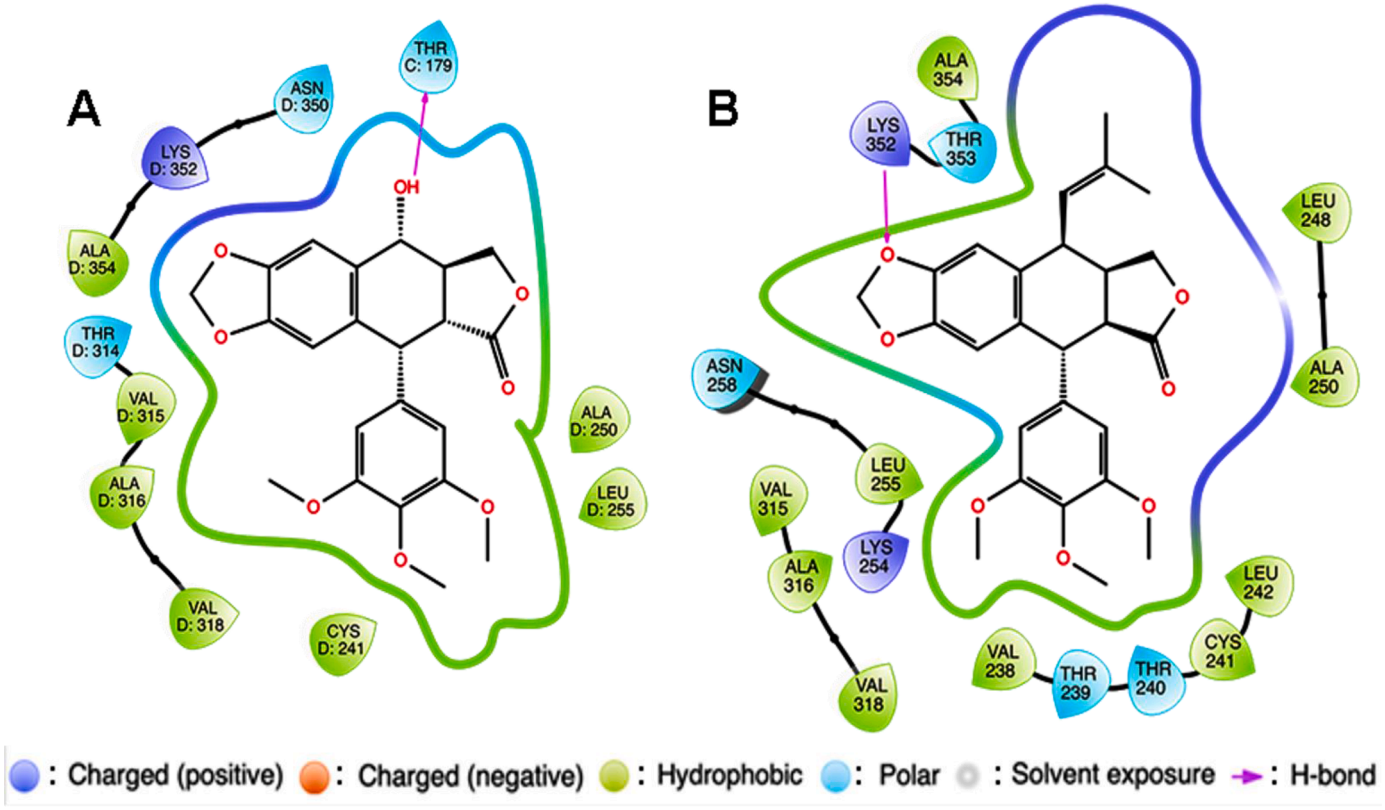


**Fig. 11. 2D-maps showing the contacts for POD (A) and S.71 (B) docked in the colchicine site of the α-β tubulin heterodimer.** Colored circles indicate types of interaction and arrows mark H-bonds. Letters C and D are associated with amino acids in fig. A, and correspond to α and β tubulin chains, respectively.

## 4. Discussion

Considering that MTs and ER participate in the infection process of different RNA viruses (Mackenzie, 2005; Naghavi and Walsh, 2017), there is a lack of treatment for DENV infection since the HTA approach (Pastorino et al., 2010), it is important to obtain and evaluate molecules that could interact with any of those cellular components, in order to develop dengue antivirals with low toxicity. Thus, potent tubulin polymerization inhibitors, such as podophyllotoxin and its derivatives could be considered as potential candidates for developing drugs against the dengue disease.

In this study, S.71 and POD were effective in DENV-2 post-infection stages, specifically at 6 and 12 hpi. They produce several morphological changes in the treated cells that could be correlated with those observed cytoskeleton alterations (Rape et al., 2011). Previous studies indicate that podophyllotoxin derivatives were able to bind to α/β-tubulin subunits (Abad et al., 2012; Kamal et al., 2014). Consequently, molecular docking studies were carried out to characterize the interaction between S.71 and α/β-tubulin subunits colchicine binding-site. These findings are compatible with other results found for podophyllotoxin and some derivatives (Kamal et al., 2014). The functional assays are confirming that the treatments caused microtubule alterations and morphological changes in the cells, which it is compatible with the explanation of why the cytoskeleton maintains cell shape and facilitates mechanical-functional interactions with the outside environment (Rape et al., 2011; Vega and Solomon, 1997).

S.71 and POD on the MTs generated an ER retraction, which possibly altered the virus replication complexes. This result was evidenced by the decrease of the MFI and by changes in the dsRNA distribution pattern. Also, low numbers of copies of negative-strand RNA and a reduction of viral ENV protein were detected (See, Fig. 12).

It has been reported that treatment during 2 h with nocodazole, another tubulin polymerization inhibitor, generates ER retraction (Terasaki et al., 1986). This would explain why ENV protein and dsRNA are altered, *i.e.*, their expression decreased and the subcellular distribution changed during S.71 and POD treatment. Moreover, Reid et al., 2018 (Reid et al., 2018) showed that the synthesis of negative genomes (RNA–) occurs from 6 to 24 hpi. Additionally, they showed the translation of viral proteins at 6 to 12 hpi (Reid et al., 2018) and determined that RNA– and positive viral genomes (RNA +) are located in the ER (Marceau et al., 2016; Puschnik et al., 2017). Other microtubule inhibitors (MTIs) such as paclitaxel, colchicine and nocodazole reduced the HCV (Bost et al., 2003) and ZIKV (Sultana et al., 2018) viral infection, confirming that the cytoskeleton is important for the flaviviridae family.

It cannot be affirmed that S.71 acts as a depolymerizing agent such as podophyllotoxin or nocodazole, because it does not show the same morphological changes, nuclear alterations or MTOC detection (Rhee et al., 2009). MTIs induce cell arrest in the G2/M phase, causing destabilization in the microtubules and consequently apoptosis (Mollinedo and Gajate, 2003; Elmore, 2007; Sultana et al., 2018; Ji and Ji, 2014). Thus, it was necessary to establish whether the S.71 and POD have the capacity to activate early cell death events.

Cellular alterations could not be attributed to an early event of cell

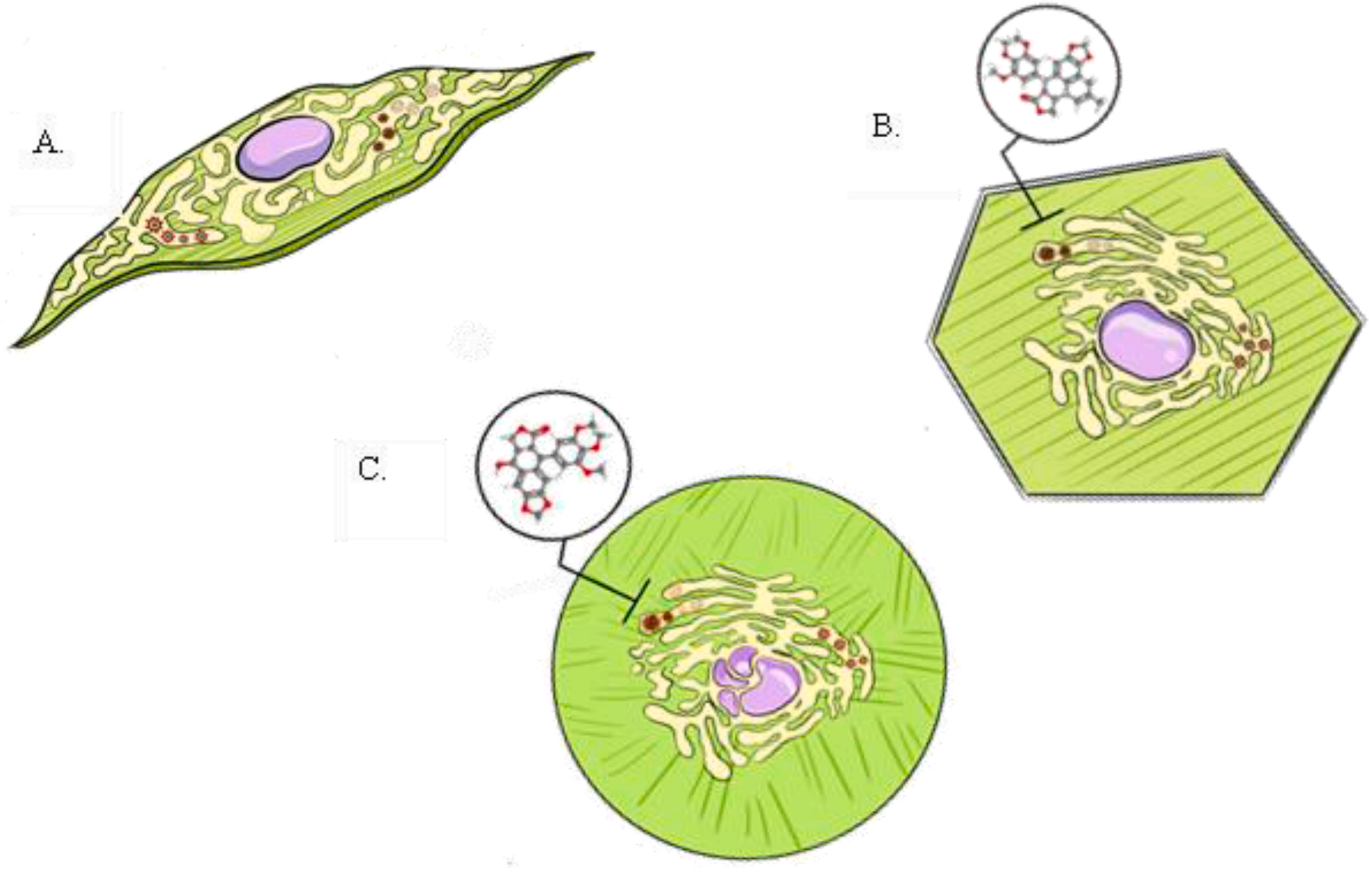


**Fig. 12. Mechanism of action of the lignan S.71**. MTs are represented by straight lines and their distribution coincides with that of the ER. **A**: DENV-2 infected cell with MTs and ER distributions similar to those of the uninfected cell, but with convoluted membranes (CM), vesicular packages (VPS), and assembled viruses constituted in the ER. **B**: Infected cell treated with S.71 showing its polygonal flat morphology, separated MTs, ER retraction, and normal nucleus. It is also suggested that this compound has a certain effect on the synthesis of negative chains and the translation of viral polyprotein; therefore, CM and VPs inhibition is indicated. **C**: Infected cell treated with POD showing its round flat morphology with fragmented MTs and pyknotic or busted nuclei. Consequently, S.71 and POD have the same antiviral effect, but the morphological alterations induced by POD treatment are dramatic, probably due to its higher cytotoxicity.

death (Fig. 8), because there was no phosphatidylserine exposure. In contrast to other POD derivatives, we highlight that the S.71 derivative does not induce cell death after 24 h of treatment (Ji and Ji, 2014). Additionally, cells treated for 24 h recovered their normal morphology three days after the treatments were removed (Fig 0.9). This finding could be the consequence of the reversible tubulin-ligand binding derived from hydrophobic interactions.

Following Lipinski's rule of five, the S.71 molecule was shown to have drug-likeness properties according to SwissADME and Osiris predictors (Elmore, 2007). The approved MTIs have low bioavailability due to their interaction with different cytochromes and efflux transporters (p-GP) (Finch and Pillans, 2014). However, in combination with other drugs, emulsions, and nanocapsules, the bioavailability can be improved (Chu et al., 2008).

Moreover, the SwissADME predicted that S.71 could be metabolized by cytochrome CYP1A2 ((Evrogen pmKate2-ER (CAT.# FP324) 2019, Ghodke-Puranik and Lamba, 2017)). Additionally, the platform described that S.71 would not have an affinity for p-GP, and could be absorbed in the gastrointestinal tract and the blood-brain barrier (Pardridge, 2012). This finding is important since some flaviviruses could invade the Central Nervous System and S.71 could eventually be a candidate to control such infections (Maximova and Pletnev, 2018).

POD is an approved drug for topical applications only due to drastic gastrointestinal effects and low bioavailability. The ADME prediction shows that POD is not a substrate of p-GP, but can be metabolized by different cytochromes CYP1A2, CYP2C19, and CYP2C9. This suggests that POD can be degraded without the possibility of being absorbed.

In previous investigations, S.71 was active against *Leishmania infantum* through tubulin polymerization inhibition. It seems possible that the aliphatic alkenyl substituent at position C-7 could be associated with biological activity and low cytotoxic effects (Escudero-Martínez et al., 2017). We prove that S.71 can control dengue infection during the first 24 hpi. Also, the differences in cytotoxicity and morphological alterations caused by S.71 and POD, allow us to hypothesize that S.71 probably does not induce substantial depolymerization of MTs. The literature and these data demonstrate that compounds with broad-spectrum biological activities are important for the treatment of several pathologies, including emerging and re-emerging viral diseases.

## Author statement

For research articles with several authors, a short paragraph specifying their individual contributions must be provided. The following statements should be used "Conceptualization, Gallego-Gómez Juan Carlos, Miranda-Brand Yaneth, Roa-Linares Vicky M and Arturo San Feliciano, Esther del Olmo; methodology, Miranda-Brand Yaneth, Carolina Santiago-Dugarte.; formal analysis, Miranda-Brand Yaneth, Carolina Santiago-Dugarte.; investigation, Miranda-Brand Yaneth.; writing—original draft preparation, Miranda-Brand Yaneth.; writing—review and editing, Miranda-Brand Yaneth and Roa-Linares Vicky M.; visualization, Betancur-Galvis Liliana, José Luis López-Pérez.; supervision Arturo San Feliciano, Gallego-Gómez Juan Carlos and Betancur-Galvis Liliana,; project administration, Betancur-Galvis Liliana. All authors have read and agreed to the published version of the manuscript."

## Declaration of Competing Interest

The authors declare that they have no known competing financial interests or personal relationships that could have appeared to influence the work reported in this paper.

## Data availability

The authors do not have permission to share data.

## Acknowledgements

JLL-P thanks SENACYT of Panama for an SNI Stimulus Awar. Additionally, YMB, VR-L and LB-G thank the financial support from CODI /Grant 2014–1041.

## Supplementary materials

Supplementary material associated with this article can be found, in the online version, at doi:10.1016/j.virusres.2022.198995.

## References

Dengue y dengue grave 2021 [Available from: https://www.who.int/es/news-room/fact-sheets/detail/dengue-and-severe-dengue].
Pastorino, B., Nougairede, A., Wurtz, N., Gould, E., de Lamballerie, X., 2010. Role of host cell factors in flavivirus infection: implications for pathogenesis and development of antiviral drugs. Antiviral Res. 87 (3), 281–294.
Greber, U.F., Way, M., 2006. A superhighway to virus infection. Cell 124 (4), 741–754.
Shrivastava, N., Sripada, S., Kaur, J., Shah, P.S., Cecilia, D, 2011. Insights into the internalization and retrograde trafficking of Dengue 2 virus in BHK-21 cells. PLoS ONE 6 (10), e25229.
Karp, G., 2009. Biología Celular y molecular, Conceptos y Experimentos, 6 ed. Mcgraw Hill, México.
Gillespie, L.K., Hoenen, A., Morgan, G., Mackenzie, J.M., 2010. The endoplasmic reticulum provides the membrane platform for biogenesis of the flavivirus replication complex. J. Virol. 84 (20), 10438–10447.
Chatel-Chaix, L., Bartenschlager, R., 2014. Dengue virus- and hepatitis C virus-induced replication and assembly compartments: the enemy inside–caught in the web. J. Virol. 88 (11), 5907–5911.
Reid, D.W., Campos, R.K., Child, J.R., Zheng, T., Chan, K.W.K., Bradrick, S.S., et al., 2018. Dengue Virus Selectively Annexes Endoplasmic Reticulum-Associated Translation Machinery as a Strategy for Co-opting Host Cell Protein Synthesis. J. Virol. 92 (7).
Paul, D., Romero-Brey, I., Gouttenoire, J., Stoitsova, S., Krijnse-Locker, J., Moradpour, D., et al., 2011. NS4B self-interaction through conserved C-terminal elements is required for the establishment of functional hepatitis C virus replication complexes. J. Virol. 85 (14), 6963–6976.
Mackenzie, J., 2005. Wrapping things up about virus RNA replication. Traffic 6 (11), 967–977.
Ayres, D.C., Loike, J.D., 1990. Lignans. Chemical, Biological and Clinical Properties. Cambridge University Press, London.
Petersen, M., Hans, J., Matern, U., 2010. Biosynthesis of phenylpropanoids and related compounds. Annu. Plant Rev. 40, 182–257. https://doi.org/10.1002/9781444320503.ch4.
Cunha, W.R., Andrade e Silva, M.L., Veneziani, R.C.S., Ambrosio, S.R., Bastos, J.K., 2012. Lignans: chemical and Biological Properties. Chp. 10, pgs 210-234. In: Rao, V. (Ed.), Phytochemicals: A Global Perspective of Their Role in Nutrition and Health. InTech, Rijeka, Croatia.
Záleśák, F., Bon, D.J.D., Pospíšil, J., 2019. Lignans and neolignans: plant secondary metabolites as a reservoir of biologically active substances. Pharmacol. Res. 146, 104284 https://doi.org/10.1016/j.phrs.2019.104284.
Xu, H., Lu, M., Tian, X., 2009. A Review on hemisynthesis, biosynthesis, biological activities, mode of action, and structure-activity relationship of podophyllotoxins: 2003-2007. Curr. Med. Chem. 16, 327–349. https://doi.org/10.2174/092986709787002682.
Cui, Q., Du, R., Liu, M., Rong, L., 2020. Lignans and their derivatives from plants as antivirals. Molecules 25, 183–199. https://doi.org/10.3390/molecules25010183.
Bertolotti, A.C., Milpied, F.B., Dupin, N., Huiart, L., Derancourt, C., 2020. Local Management of Anogenital Warts in Non-Immunocompromised Adults: a Network Meta-Analysis of Randomized Controlled Trials. Dermatol. Ther. 10, 249–262. https://doi.org/10.1007/s13555-020-00357-z.
Attiaa, A.M., Bakreya, O.A., Fakhrey, S.M., El-Motalebb, A., 2015. The use of podophyllotoxin for treatment of genital warts. Menoufia Med. J. 28, 367–371. https://doi.org/10.4103/1110-2098.163886.
Gordaliza, M., García, P.A., del Corral, J.M., Castro, M.A., Gómez-Zurita, M.A., 2004. Podophyllotoxin: distribution, sources, applications and new cytotoxic derivatives. Toxicon 44, 441–459. https://doi.org/10.1016/j.toxicon.2004.05.008.
Hande, K.R., 1998. Etoposide: four decades of development of a topoisomerase II inhibitor. Eur. J. Cancer. 34 (10), 1514–1521. https://doi.org/10.1016/S0959-8049(98)00228-7.
Montecucco, A., Zanetta, F., Biamonti, G., 2015. Molecular Mechanisms of Etoposide. XCLI J. 14, 95–108. https://doi.org/10.17179/excli2014-561.
Gordaliza, M., Castro, M.A., García-Grávalos, M.D., Ruiz, P., Miguel del Corral, J.M., San Feliciano, A., 1994. Antineoplastic and antiviral activities of podophyllotoxin related lignans. Arch. Pharm. 327, 175–179. https://doi.org/10.1002/ardp.19943270309.
Sudo, K., Konno, K., Shigeta, S., Yokota, T., 1998. Inhibitory effects of podophyllotoxin derivatives on herpes simplex virus replication. Antivir. Chem. Chemother. 9, 263–267. https://doi.org/10.1177/095632029800900307.
Cohen, T., Schwarz, T.M., Vigant, F., Gardner, T.J., Hernandez, R.E., Lee, B., Tortorella, D., 2016. The microtubule inhibitor podofilox inhibits an early entry step of human cytomegalovirus. Viruses 8, 295. https://doi.org/10.3390/v8100295.

Hernández, A.P., Díez, P., García, P.A., Miguel del Corral, J.M., Pérez-Andrés, M., Díez, D., San Feliciano, A., Fuentes, M., Castro, M.A, 2018. New hybrids derived from podophyllic aldehyde and diterpenylhydroquinones with selectivity toward osteosarcoma cells. ACS Med. Chem. Lett. 9, 328–333. https://doi.org/10.1021/acsmedchemlett.7b00493.

Abad, A., López-Pérez, J.L., del Olmo, E., García-Fernández, L.F., Francesch, A., Trigili, C., Barasoain, I., Andreu, J.M., Díaz, J.F., 2012. San Feliciano A. Synthesis and antimitotic and tubulin interaction profiles of novel pinacol derivatives of podophyllotoxins. J. Med. Chem. 55, 6724–6737. https://doi.org/10.1021/jm2017573 (*and references therein*).

Evrogen pmKate2-ER (CAT.# FP324) 2018 [Available from: http://evrogen.com/products/vectors/pmKate2-ER/pmKate2-ER.shtml.

Roa-Linares, V.C., Brand, Y.M., Agudelo-Gomez, L.S., Tangarife-Castano, V., Betancur-Galvis, L.A., Gallego-Gomez, J.C., et al., 2016. Anti-herpetic and anti-dengue activity of abietane ferruginol analogues synthesized from (+)-dehydroabietylamine. Eur. J. Med. Chem. 108, 79–88.

Cardozo, F.T., Camelini, C.M., Mascarello, A., Rossi, M.J., Nunes, R.J., Barardi, C.R., et al., 2011. Antiherpetic activity of a sulfated polysaccharide from Agaricus brasiliensis mycelia. Antiviral Res.

Martinez-Gutierrez, M., Castellanos, J.E., Gallego-Gomez, J.C., 2011. Statins reduce dengue virus production via decreased virion assembly. Intervirology 54 (4), 202–216.

Castillo, J.A., Castrillon, J.C., Diosa-Toro, M., Betancur, J.G., St Laurent 3rd, G.,., Smit, J. M., et al., 2016. Complex interaction between dengue virus replication and expression of miRNA-133a. BMC Infect. Dis. 16, 29.

Castellanos, J.E., Neissa, J.I., Camacho, S.J., 2016. Dengue virus induces apoptosis in SH-SY5Y human neuroblastoma cells. Biomedica 36 (0), 156–158.

Friesner, R.A., Banks, J.L., Murphy, R.B., Halgren, T.A., Klicic, J.J., Mainz, D.T., et al., 2004. Glide: a new approach for rapid, accurate docking and scoring. 1. Method and assessment of docking accuracy. J. Med. Chem. 47 (7), 1739–1749.

Friesner, R.A., Murphy, R.B., Repasky, M.P., Frye, L.L., Greenwood, J.R., Halgren, T.A., et al., 2006. Extra precision glide: docking and scoring incorporating a model of hydrophobic enclosure for protein-ligand complexes. J. Med. Chem. 49 (21), 6177–6196.

Halgren, T.A., Murphy, R.B., Friesner, R.A., Beard, H.S., Frye, L.L., Pollard, W.T., et al., 2004. Glide: a new approach for rapid, accurate docking and scoring. 2. Enrichment factors in database screening. J. Med. Chem. 47 (7), 1750–1759.

Naghavi, M.H., Walsh, D., 2017. Microtubule Regulation and Function during Virus Infection. J. Virol. 91 (16), 1–17.

Rape, A., Guo, W.H., Wang, Y.L., 2011. Microtubule depolymerization induces traction force increase through two distinct pathways. J. Cell Sci. 124 (Pt 24), 4233–4240.

Kamal, A., Srinivasa Reddy, T., Polepalli, S., Shalini, N., Reddy, V.G., Subba Rao, A.V., et al., 2014. Synthesis and biological evaluation of podophyllotoxin congeners as tubulin polymerization inhibitors. Bioorg. Med. Chem. 22 (19), 5466–5475.

Sultana, F., Reddy Bonam, S., Reddy, V.G., Nayak, V.L., Akunuri, R., Rani Routhu, S., Alarifi, A., Halmuthur, M.S.K., Kamal, A., 2018. Synthesis of benzo[d]imidazo[2,1-b]thiazole-chalcone conjugates as microtubule targeting and apoptosis inducing agents. Bioorg. Chem. 76, 1–12. https://doi.org/10.1016/j.bioorg.2017.10.019.

Terasaki, M., Chen, L.B., Fujiwara, K., 1986. Microtubules and the endoplasmic reticulum are highly interdependent structures. J. Cell Biol. 103 (4), 1557–1568.

Bost, A.G., Venable, D., Liu, L., Heinz, B.A., 2003. Cytoskeletal requirements for hepatitis C virus (HCV) RNA synthesis in the HCV replicon cell culture system. J. Virol. 77 (7), 4401–4408.

Marceau, C.D., Puschnik, A.S., Majzoub, K., Ooi, Y.S., Brewer, S.M., Fuchs, G., et al., 2016. Genetic dissection of Flaviviridae host factors through genome-scale CRISPR screens. Nature 535 (7610), 159–163.

Puschnik, A.S., Marceau, C.D., Ooi, Y.S., Majzoub, K., Rinis, N., Contessa, J.N., et al., 2017. A small molecule oligosaccharyltransferase inhibitor with pan-flaviviral activity. Cell Rep. 21 (11), 3032–3039.

Rhee, D.Y., Zhao, X.Q., Francis, R.J., Huang, G.Y., Mably, J.D., Lo, C.W., 2009. Connexin 43 regulates epicardial cell polarity and migration in coronary vascular development. Development 136 (18), 3185–3193.

Mollinedo, F., Gajate, C., 2003. Microtubules, microtubule-interfering agents and apoptosis. Apoptosis 8 (5), 413–450.

Elmore, S., 2007. Apoptosis: a review of programmed cell death. Toxicol. Pathol. 35 (4), 495–516. https://doi.org/10.1080/01926230701320337.

Elmore, S., 2007. Apoptosis: a review of programmed cell death. Toxicol Pathol 35 (4), 495–516.

Sultana, F., Reddy Bonam, S., Reddy, V.G., Nayak, V.L., Akunuri, R., Rani Routhu, S., et al., 2018. Synthesis of benzo[*d*]imidazo[2,1-b] thiazole-chalcone conjugates as microtubule targeting and apoptosis-inducing agents. Bioorg. Chem. 76, 1–12.

Ji, C.F., Ji, Y.B., 2014. Apoptosis of human gastric cancer SGC-7901 cells induced by podophyllotoxin. Exp. Ther. Med. 7 (5), 1317–1322.

Finch, A., Pillans, P., 2014. P-glycoprotein and its role in drug-drug interactions. | Aust. Prescr. 37, 137–139.

Chu, Z., Chen, J.S., Liau, C.T., Wang, H.M., Lin, Y.C., Yang, M.H., et al., 2008. Oral bioavailability of a novel paclitaxel formulation (Genetaxyl) administered with cyclosporin A in cancer patients. Anticancer Drugs 19 (3), 275–281.

Ghodke-Puranik, Y.A., Lamba, J.K., 2017. Chapter 7 - Pharmacogenomics. In: Patwardhan, B, Chaguturu, R (Eds.), Innovative Approaches in Drug Discovery. Academic Press, Boston, pp. 195–234.

Pardridge, W.M., 2012. Drug transport across the blood-brain barrier. J. Cereb. Blood Flow Metab. 32 (11), 1959–1972.

Maximova, O.A., Pletnev, A.G., 2018. Flaviviruses and the Central Nervous System: revisiting Neuropathological Concepts. Annu. Rev. Virol. 5 (1), 255–272.

Escudero-Martínez, J.M., et al., 2017. Antileishmanial activity and tubulin polymerization inhibition of podophyllotoxin derivatives on Leishmania infantum. Drugs and Drug Resistance 7, 272e285.

Vega, L.R., Solomon, F., 1997. Microtubule function in morphological differentiation: growth zones and growth cones. Cell 6, 825–828.